



Cite this: DOI: 10.1039/c9dt03902c

Synthesis and antiproliferative activity of benzimidazole-based, trinuclear neutral cyclometallated and cationic, N[^]N-chelated ruthenium(II) complexes†

Athi Welsh,^a Laa-iqa Rylands,^a Vladimir B. Arion,^b Sharon Prince^c and Gregory S. Smith^{*a}

A series of 2-phenyl and 2-pyridyl tris-benzimidazole ligands was reacted with the [Ru(*p*-cymene)Cl₂]₂ dimer to yield the corresponding neutral cyclometallated and cationic organoruthenium(II) complexes. All of the synthesized compounds were characterized using an array of spectroscopic and analytical techniques, including ¹H, ¹³C nuclear magnetic resonance (NMR), infrared spectroscopy and mass spectrometry. The trinuclear compounds were screened for their cytotoxicity against the MCF-7 breast cancer cell line and the triple negative MDA-MB-231 breast cancer cell line at concentrations of 10 and 20 μM. Overall, the 2-pyridyl ligands **10** and **11**, and their corresponding trinuclear complexes **[16][PF₆]₃** and **[17][PF₆]₃**, show the most promising activity as these compounds significantly reduce the percentage cell survival of MCF-7 and MDA-MB-231 breast cancer cell lines at the aforementioned fixed concentrations. It was observed that **10** and **[16][PF₆]₃** show potency greater than that of cisplatin against the MCF-7 breast cancer cell line, and **[17][PF₆]₃** shows potency comparable to that of cisplatin against the MCF-7 cell line. Additionally, the synthesized compounds were observed to have relatively low cytotoxicity towards MCF-12A breast epithelial cells and relatively higher selectivity towards MCF-7 breast cancer cells compared to cisplatin.

Received 2nd October 2019,
Accepted 13th December 2019

DOI: 10.1039/c9dt03902c

rsc.li/dalton

Introduction

Cancer is a non-communicable disease that causes abnormal cell growth and division, and remains one of the major causes of death globally,¹ affecting the lives of approximately 600 000 people.^{2,3} The defining characteristic of cancer is the abrupt evolution of abnormal cells which overgrow, and may spread *via* metastasis to other organs using either the lymphatic system or bloodstream.⁴ Despite improvements in chemotherapy treatments, the development of resistance remains the main cause of chemotherapy failure.

The prevalence of the benzimidazole core in biologically active molecules has stimulated systematic investigations of this class of heterocyclic compounds. It is well established that

benzimidazole derivatives show an array of biological activity, including antiviral, antihistaminic, antiparasitic, antimalarial and anticancer activity.^{5,6} Due to their vast medicinal value, the research of benzimidazole-containing drugs is an active and attractive field in chemistry. Based on the success of clinically approved benzimidazole derivatives, such as omeprazole, lansoprazole and albendazole, research focussing on the medicinal use of benzimidazoles as chemotherapeutic agents remains promising,⁷ with several recent publications reporting benzimidazole derivatives with various substitution patterns, possessing potent anticancer activities.^{7,8}

The fortuitous discovery of *cis*-dichlorodiammineplatinum(II), commonly known as cisplatin, by Rosenberg in 1967 paved the way for the development of organometallic complexes as an alternative class of chemotherapeutic agents. Today, platinum-based drugs, cisplatin, carboplatin and oxaliplatin, constitute as much as 70% of cancer treatment regimens.⁹ However, their use is limited by their severe side effects and the development of resistance by numerous cancers. Efforts to target resistance has resulted in a shift towards the development of other platinum-group metals (PGMs) as potential anticancer metallodrugs.¹⁰

By far, ruthenium-based drugs have been very successful in this category as they offer more potential as cytostatic and

^aDepartment of Chemistry, University of Cape Town, Rondebosch 7701, Cape Town, South Africa. E-mail: Gregory.Smith@uct.ac.za

^bInstitute of Inorganic Chemistry of the University of Vienna, Währinger Strasse 42, 1090 Vienna, Austria

^cDepartment of Human Biology, University of Cape Town, Faculty of Health Science, Observatory 7925, South Africa

† Electronic supplementary information (ESI) available. CCDC 1940327 and 1940326. For ESI and crystallographic data in CIF or other electronic format see DOI: 10.1039/c9dt03902c

cytotoxic agents with novel modes of action.¹¹ Indeed, ruthenium complexes have gained significant prominence as potential anticancer agents, as they display diverse and non-conventional mechanisms of action.¹² These ruthenium complexes offer a range of oxidation states which are accessible under physiological conditions, which is unique among PGMs. This feature offers a unique advantage in rational drug design as the anticancer activity of most metal-based compounds is dependent on the metal's oxidation state.^{13–16} To date, the most successful ruthenium complexes are the New Anti-tumour Metastatic Inhibitor-A (NAMI-A) and IT-139 which have entered clinical trials.^{9,17} NAMI-A has minimal effects on primary tumour growth¹⁸ but has anti-metastatic properties. Indeed, it can reduce metastatic mass and prevent the formation of secondary tumours. On the other hand, IT-139 is a cytotoxic agent that is effective against advanced solid tumours, showing promising activity against non-small lung cancer, neuroendocrine and sarcoma tumours.¹⁸ The success of ruthenium complexes and their alternate mechanisms of action suggest that they may facilitate the discovery of new combination chemotherapy agents. There have been several reports of half-sandwich ruthenium(II)-arene complexes which have several intracellular targets. These targets include DNA interaction and binding,¹⁹ inhibition of enzymes which are overexpressed in human cancers including the PARP-1,²⁰ CDK1,²¹ and cathepsin B enzymes,²² which are known to play vital roles in the proliferation and progression of cancers, and lastly, induction of apoptosis.^{23,24}

The success of mononuclear chemotherapeutic agents also pre-empted the investigation of multinuclear PGM complexes as potential drug candidates. This interest was initiated by the observation that compounds bearing more than one metal center have improved biological activities relative to their mononuclear counterparts.^{25–27} The improved cytotoxicity of multinuclear macromolecules may also be attributed to the enhanced permeability and retention (EPR) effect.^{25,28} This is a phenomenon in which solid tumours have defective and permeable blood vessels, to ensure a sufficient supply of nutrients and oxygen to tumour tissues for rapid growth. Macromolecules, such as polynuclear complexes, exploit this EPR effect and selectively accumulate in tumour cells.²⁹ The most successful trinuclear candidate is BBR3464, which comprises three platinum(II) centres bridged by a polyamine scaffold. The polyamine scaffold, and multinuclearity of the complex results in a slightly different mechanism when interacting with DNA, as the complex spans a long distance along DNA strands.¹⁰ The complex is currently in phase II clinical trials for the treatment of melanoma, lung, ovarian and gastric tumours.³⁰ However, the study of transition metals, such as ruthenium, for the preparation of polynuclear complexes opens another manifold of diversity.³¹

The incorporation of multivalent pharmacophores and the combination of these ligands with PGMs, to form trinuclear complexes, is a prolific area of research which we have previously explored as a strategy in anticancer drug design.^{32–36} This study explored triruthenium(II) complexes based on benzimidazole motifs anchored on a tris-2-(ethylamino)amine

scaffold, which were investigated for their potential anticancer activity against two breast cancer cell lines, the MCF-7 and MDA-MB-231 cell lines. The focus on breast cancer was a result of recent GLOBOCAN statistics which estimate that in women, breast cancer is the most commonly diagnosed cancer (11.6% of the total new cases) and the leading cause of cancer-related mortality (6.6% of total cancer deaths). In both sexes combined, the only cancer that has a slightly higher number of new diagnoses and cancer related mortalities is lung cancer, closely followed by breast cancer.³⁷

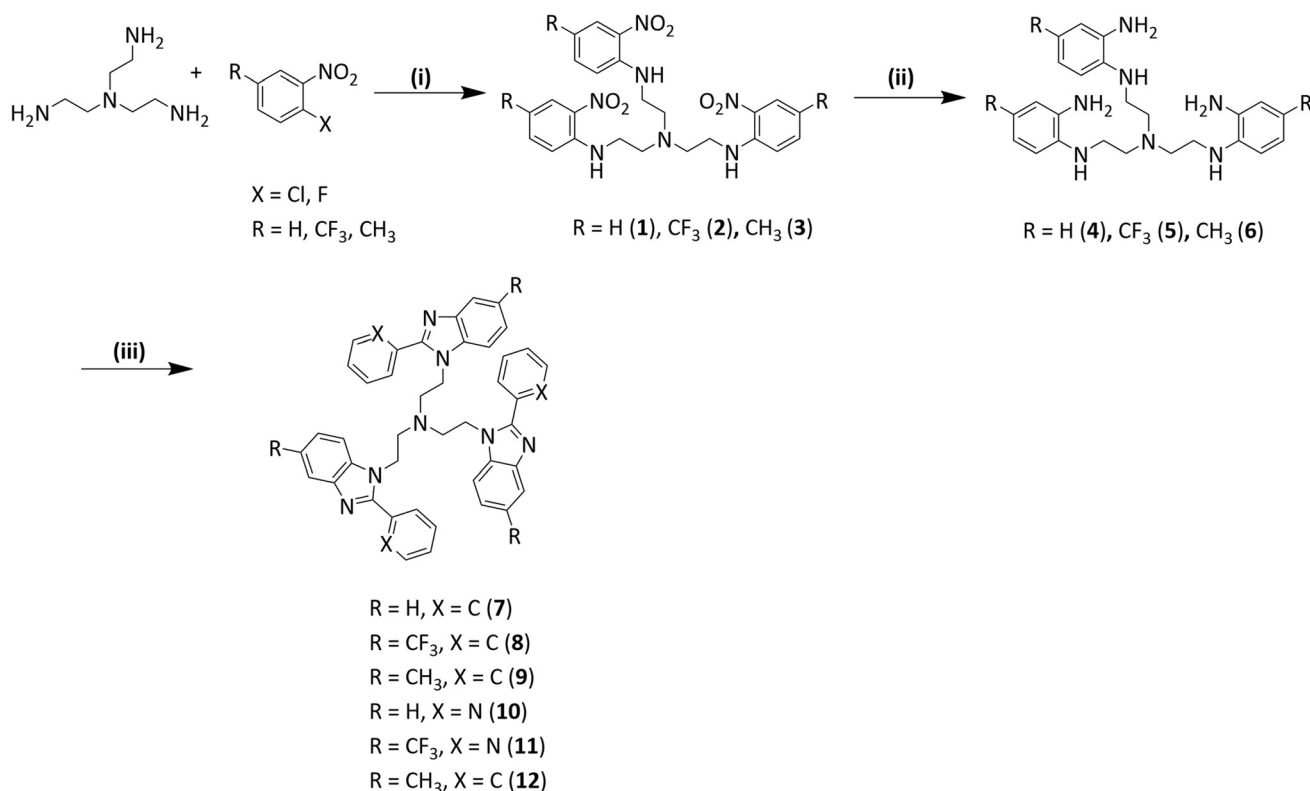
Results and discussion

Synthesis of 2,5-disubstituted tris-benzimidazole ligands (7–12)

The synthesis of the 2,5-disubstituted tris-benzimidazoles (7–12) involved three steps: (i) a nucleophilic aromatic substitution reaction (S_NAr) of tris(2-aminoethyl)amine with either *ortho*-substituted fluoro- or chloro-nitrobenzenes (ii) the reduction of the nitro-functionalities to primary amines, and lastly (iii) the condensation–cyclisation with either benzaldehyde or 2-pyridinecarboxaldehyde to afford the desired tris-benzimidazole ligand (Scheme 1).

The pure ligands were isolated as coloured solids in moderate to good yields (33–71%) and are soluble in several polar organic solvents including ethanol, acetone and dimethylsulfoxide. Comparison of the ¹H NMR spectra of the 2-phenyl (7–9) and 2-pyridyl tris-benzimidazole ligands (10–12) and their corresponding tris-1,2-benzenediamines (4–6) revealed several notable features. Firstly, the ¹H NMR spectra of the benzimidazole ligands did not possess any significant changes in the aliphatic region, as two aliphatic signals are observed, corresponding to the methylene protons on the tris-core. However, in the aromatic region, additional aromatic signals are observed, and these additional signals collectively integrate for either fifteen (for the 2-phenyl tris-benzimidazole ligands 7–9) or twelve protons (for the 2-pyridyl tris-benzimidazole ligands 10–12). These additional aromatic signals correspond to the protons of either the 2-phenyl or 2-pyridyl functionalities on the 2-position of the benzimidazole motifs and are indicative of successful synthesis of the benzimidazole entity. In the IR spectra of the 2-phenyl benzimidazoles (7–9), one absorption band between 1695–1625 cm⁻¹ was observed and this absorption band corresponds to the imine (C=N) bond stretch. The IR spectra of the 2-pyridyl tris-benzimidazole ligands (10–12) revealed two absorption bands, one in the range 1592–1733 cm⁻¹ and another in the range 1489–1587 cm⁻¹, that correspond to imine (C=N) bond stretches of the benzimidazole motif and the C=N bond stretch in 2-pyridyl functionality, respectively.

The molecular structures for compounds 7 and 8 were confirmed in the solid state by single crystal X-ray diffraction, with molecular structures depicted in Fig. 1 and 2, respectively. Single crystals of 7 and 8 were obtained by slow diffusion of a concentrated solution of either 7 or 8 in dichloromethane layered with ethyl acetate, at room temperature. Further crystal-



Scheme 1 Reagents and conditions: (i) DMF/RT/24 h; (ii) $\text{NH}_4\text{Cl}/\text{Zn}/\text{MeOH}/\text{RT}/1$ h; (iii) benzaldehyde/EtOH/TFA/80 °C/24 h or 2-pyridinecarboxaldehyde/EtOH/TFA/RT/24 h.

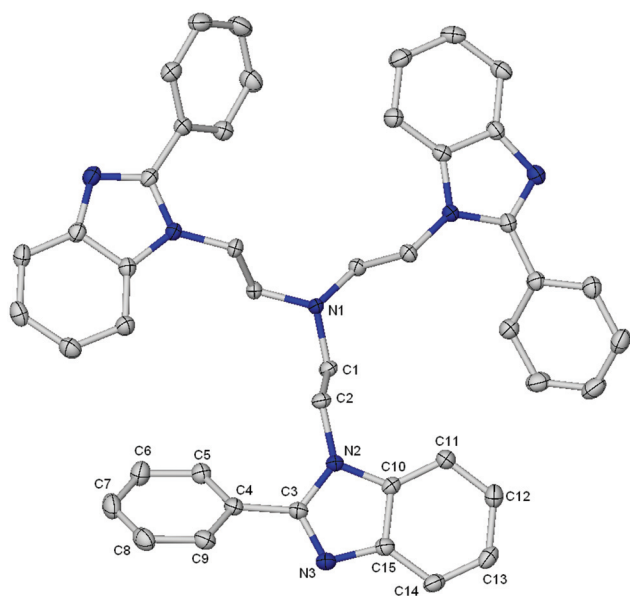


Fig. 1 The ORTEP drawing of the molecular structure of compound **7**, hydrogen atoms have been omitted for clarity. Thermal ellipsoids are at the 50% probability level.

lographic data and refinement parameters for the two ligands are summarised in Table 1. The compounds **7** and **8** crystallised in the trigonal space group $P\bar{3}c1$ and triclinic space group

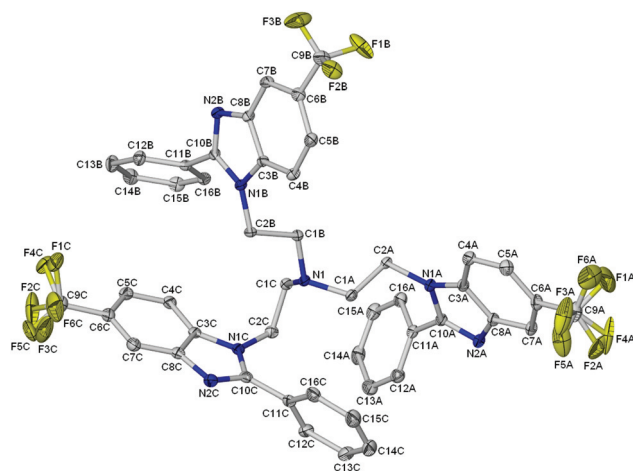


Fig. 2 The ORTEP drawing of the molecular structure of compound **8**, hydrogen atoms have been omitted for clarity. Thermal ellipsoids are at the 50% probability level.

$P\bar{1}$, respectively. In **8**, the F atoms of two of the three trifluoromethyl groups (C9A and C9C) are disordered over two sites, with refined site occupancy factors of 0.615(15) for F1A, F2A and F3A, 0.315(15) for F4A, F5A and F6A, 0.778(9) for F1C, F2C and F3C, 0.222(9) for F4C, F5C and F6C. The imine (C=N) bond lengths in the benzimidazole cores of **7** and **8** range

Table 1 Crystallographic data for compounds **7** and **8**

	Compound 7	Compound 8
Empirical formula	C ₄₅ H ₃₉ N ₇	C ₄₈ H ₃₆ F ₉ N ₇
Formula weight	677.83	881.85
Temperature (K)	173(2)	173(2)
Crystal system	Trigonal	Triclinic
Space group	<i>P</i> $\bar{3}c1$	<i>P</i> $\bar{1}$
<i>a</i> (Å)	15.9799(10)	12.9590(8)
<i>b</i> (Å)	15.9799(10)	13.5286(10)
<i>c</i> (Å)	15.7925(9)	14.2464(10)
α (°)	90	70.930(2)
β (°)	90	64.023(2)
γ (°)	120	81.799(2)
Volume (Å ³)	3492.4(5)	2122.1(3)
<i>Z</i>	4	2
ρ_{calc} (g cm ⁻³)	1.289	1.380
μ (mm ⁻¹)	0.078	0.111
<i>F</i> (000)	1432.0	908.6
Crystal size (mm ³)	0.44 × 0.26 × 0.25	0.18 × 0.18 × 0.12
Radiation	MoK α (λ = 0.71073)	MoK α (λ = 0.71073)
2 θ range for data collection (°)	2.942 to 56.514	3.18 to 56.62

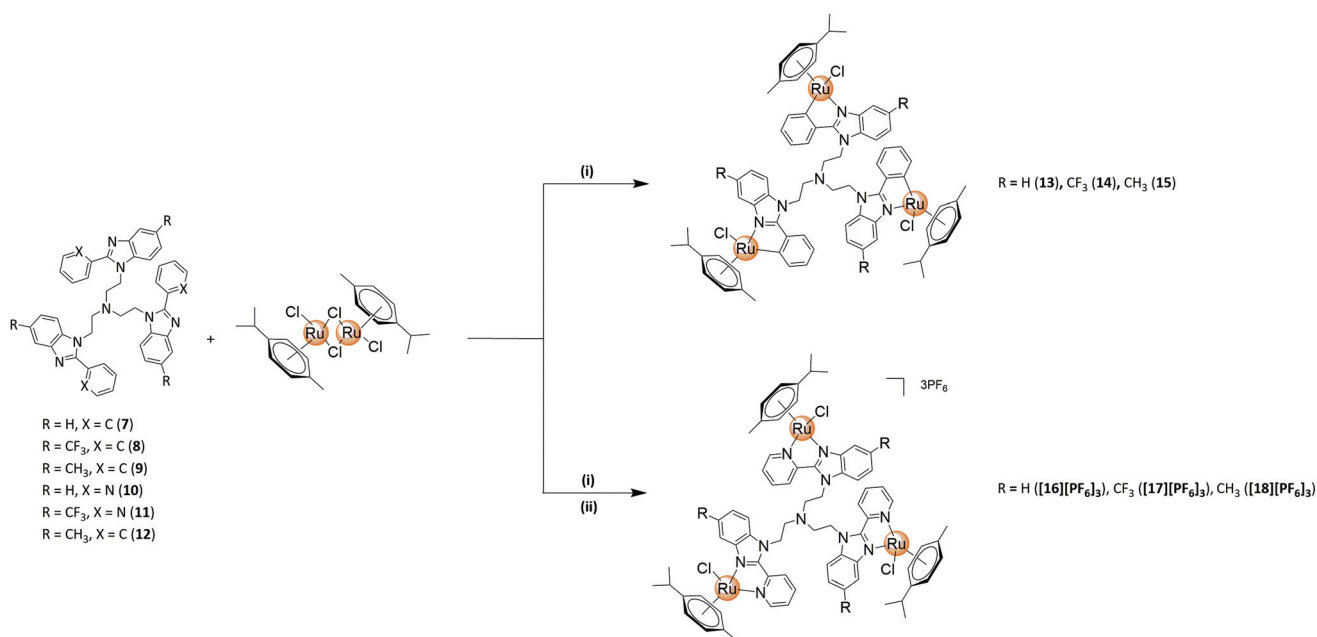
from 1.317 Å to 1.320 Å and are comparable to imine bond lengths observed in the literature for analogous 2-phenyl benzimidazole compounds.^{38,39}

Synthesis of neutral cyclometallated trinuclear C[∧]N-Ru(η)-*p*-cymene complexes (**13**–**15**)

Generally, the trinuclear cyclometallated complexes were synthesized *via* a C–H activation reaction, in which the

appropriate 2-phenyl tris-benzimidazole ligand (**7**–**9**) was reacted with the [Ru(*p*-cymene)Cl₂]₂ dimer in the presence of sodium acetate (Scheme 2). The compounds **13**–**15** were isolated in excellent yields (84–88%) as green (**13**) or dark yellow powders (**14** and **15**) that are air- and moisture-stable, and are soluble in dimethylsulfoxide, acetonitrile or acetone.

In the ¹H NMR spectra of **13**–**15**, the appearance of four (for **13**) or five (for **14** and **15**) signals between 5.0 and 6.0 ppm which collectively correspond to the aromatic protons of the *p*-cymene ring, confirm successful cyclometallation. The appearance of two multiplets in the range 0.5–1.0 ppm is due to the methyl protons of the iso-propyl functionality on the *p*-cymene ring. These signals suggest that the methyl protons are in electronically distinct environments and thus further corroborating successful cyclometallation. The difference in electronic environments may be attributed to the stereogenic metal centers induced upon cyclometallation. High-resolution mass spectrometry analysis of **14** revealed an ion peak at *m/z* = 1157.3227 corresponding to the fragment [M + Na⁺ – C₂₆H₂₅ClF₃N₂Ru]⁺. Additionally, upon analysis of the high-resolution mass spectrum of **15**, a peak at *m/z* = 1494.3296 was observed which corresponds to the [M – Cl]⁺ ion. In the IR spectra of these complexes it is generally observed that the absorption band corresponding to the imine (C=N) bond was at a lower wavenumber, in the range of 1580–1596 cm⁻¹, relative to the corresponding 2-phenyl tris-benzimidazole ligands **7**–**9**, with imine (C=N) absorption bands between 1625 and 1695 cm⁻¹. This is due to the extensive pi-backbonding between the low-spin d⁶



Scheme 2 Reagents and conditions: For **13**–**15**: (i) MeCN or DCM : EtOH (1 : 1)/NaOAc/RT/24 h; for **16**][PF₆]₃–**18**][PF₆]₃: (i) DCM : EtOH (1 : 1)/RT/24 h; (ii) DCM : EtOH (1 : 1)/NH₄PF₆/RT/1 h.

ruthenium center and the benzimidazole motif. This synergistic strengthening of the N–Ru(II) bond and weakening of the imine C=N bond results in the observed shift in the imine (C=N) bond stretch in the complexes to a lower wavenumber.

Synthesis of cationic N^1N -Ru(II)-*p*-cymene metal complexes ([16][PF₆]₃–[18][PF₆]₃)

The synthesis of the cationic ruthenium complexes was achieved in two steps: (i) firstly, the ruthenium [Ru(η^6 -*p*-Pr¹C₆H₄Me)Cl₂]₂ dimer was reacted with the appropriate 2-pyridyl tris-benzimidazole ligand (10–12), followed by (ii) an anion exchange reaction with ammonium hexafluorophosphate (Scheme 2). The complexes [16][PF₆]₃–[18][PF₆]₃ were isolated in moderate to good yields (51–75%) as yellow hexafluorophosphate salts that are air- and moisture-stable, and are soluble in dimethylsulfoxide, dichloromethane or acetone.

Comparison of the ¹H NMR spectra of [16][PF₆]₃–[18][PF₆]₃ to those of the corresponding ligands 10–12, reveals a signal attributed to the proton bonded to the carbon adjacent to the pyridyl nitrogen at a significantly higher chemical shift in the ruthenium complexes [16][PF₆]₃–[18][PF₆]₃ (from 8.25–8.50 ppm in the ligands, to ~9.6 ppm in the metal complexes). This is due to the bonding of the pyridyl nitrogen to the ruthenium center resulting in pi-backbonding, which consequentially results in the reduction of electron density on the carbon adjacent to the pyridyl nitrogen. Additionally, the aromatic protons of the *p*-cymene ring were observed as either three ([16][PF₆]₃) or four signals (for [17][PF₆]₃ and [18][PF₆]₃) in the range 6.00–6.50 ppm, corroborating the coordination of the ruthenium center to both the nitrogens of the benzimidazole motif and the 2-pyridyl functionalities. These signals are indicative of the stereogenicity introduced through chelation of the Ru(II) center to the benzimidazole nitrogen and the 2-pyridyl nitrogen. Generally, the IR spectra revealed that the absorption bands corresponding to the imine (C=N) bond of the benzimidazole cores and the pyridyl C=N bond are at lower wavenumbers in the complexes [16][PF₆]₃–[18][PF₆]₃ (in the ranges 1572–1674 cm⁻¹ and 1464–1490 cm⁻¹ for the imine and pyridyl C=N bonds respectively) relative to their corresponding 2-pyridyl tris-benzimidazole ligands 10–12 (with absorption bands in the ranges 1620–1733 cm⁻¹ and 1586–1590 cm⁻¹ for the imine and pyridyl C=N bonds, respectively). Again, this lowering of absorption bands is indicative of pi-backbonding between the imine and pyridyl nitrogens to the ruthenium center, resulting in weakening of both the imine and pyridyl C=N bonds. The stability of the cationic ruthenium(II) complexes ([16][PF₆]₃–[18][PF₆]₃) was investigated using UV/Vis spectroscopy at 37 °C to simulate the chemical environment prior to cell viability studies. In the obtained UV/Vis spectra of the complexes (Fig. S35–S37†), no significant changes were noted after incubating the compounds at 37 °C for 24 and 48 h. Thus, the compounds

remain intact in DMSO and do not interact with DMSO molecules.

Synthesis of a monomeric 2-pyridylbenzimidazole ligand (19) and its corresponding cationic N^1N -Ru(II)-*p*-cymene metal complex ([20][PF₆])

Prior to the synthesis of the mononuclear 2-pyridylbenzimidazole ligand (19) and the corresponding Ru(II) complex ([20][PF₆]), results from the *in vitro* anticancer evaluation (*vide infra*) of the tris-benzimidazole ligands and complexes provided the criteria for the selection of the most active tris-benzimidazole ligand and corresponding complex (10 and [16][PF₆]₃, respectively). The synthesis of the monomeric compound 19 was carried out using the same three-step procedure as described previously for the synthesis of the 2,5-disubstituted tris-benzimidazole ligands. Analysis of the obtained ¹H NMR spectra for the *N*-ethyl-2-nitroaniline and *N*¹-ethylbenzene-1,2-diamine synthons, and the target 2-pyridylbenzimidazole ligand (19) are consistent with the proposed structures of these compounds. Additionally, the chemical shifts and signal multiplicities observed in each of the obtained ¹H NMR spectra were all comparable to those reported in literature.^{40–42}

The mononuclear cationic complex [20][PF₆] was isolated in 81% yield as the yellow hexafluorophosphate salt that is air- and moisture-stable, and is soluble in dimethylsulfoxide, dichloromethane or acetone. Comparison of the ¹H NMR spectra of [20][PF₆] to that of 19, shows the first indicator of successful complex formation, as the splitting of the signal corresponding to the methylene protons of the ethyl functionality from a distinct quartet, in 19, to an intricate multiplet, in [20][PF₆]. This splitting is due to the chiral Ru(II) center, resulting in the diastereotopicity of these methylene protons. Additionally, three signals for the aromatic protons of the *p*-cymene ancillary ligand are observed between 6.0 and 6.5 ppm. Furthermore, analysis of the high-resolution mass spectrum of [20][PF₆] revealed a peak at *m/z* = 494.0948 corresponding to the [M – PF₆]⁺ ion.

In vitro anticancer evaluation

The antiproliferative activity of the synthesized 2-phenyl and 2-pyridyl tris-benzimidazole ligands and their corresponding triruthenium(II) complexes was evaluated *in vitro* against the MCF-7 breast cancer cell line at an initial dose of 10 μM. The initial concentration was chosen based on the National Cancer Institute (NCI), which conducts a pre-screen to assess a new drug candidate at 10 μM.⁴³ Due to the compounds showing very mild to no activity at 10 μM, the concentration was subsequently doubled to 20 μM. The cytotoxicity data obtained for the tested compounds are summarized in Fig. S1† (for the 2-phenyl ligands and corresponding cyclometallated complexes) and Fig. S2† (for the 2-pyridyl ligands and corresponding cationic complexes). Cisplatin was included as a positive control at the reported IC₅₀ value of 35 μM.⁴⁴

Generally, the 2-phenyl ligands and their corresponding metal complexes show very mild to no activity at 20 μM as the 2-phenyl ligand series and corresponding cyclometallated

complexes are observed to reduce cell viability to only 78–86% (Fig. S1†). However, the 2-pyridyl ligands and corresponding complexes display slightly improved cytotoxicity (Fig. S2†) relative to their corresponding 2-phenyl counterparts. A clear indication of this is when comparing the cytotoxic activity of the unsubstituted 2-phenyl (7, with a percentage cell survival of 78%) and 2-pyridyl (10, with a percentage cell survival of 43%) ligands, and their respective cyclometallated (13, with a percentage cell survival of 86%) and cationic complexes ([16][PF₆]₃, with a percentage cell survival of 71%). The same trend was observed upon the treatment of the MCF-7 cells with 20 μM of the compounds. Selected compounds were observed to display an enhanced reduction in cell viability at 20 μM relative to the 10 μM treatment. The *in vitro* activity of the 2-phenyl ligands and their corresponding cyclometallated Ru(II) complexes (Fig. S1†) shows that the unsubstituted 2-phenyl tris-benzimidazole ligand (7) has approximately 16 and 8% greater inhibition of cell viability compared to the corresponding trinuclear cyclometallated Ru(II) complex (13) at 10 and 20 μM, respectively. However, in general, the cyclometallated complexes (14 and 15) were observed to have slightly enhanced biological activity compared to their corresponding ligands at both the tested concentrations. Analysis of the *in vitro* cytotoxic data obtained for the 2-pyridyl tris-benzimidazole ligands (10–12) and their corresponding cationic N^N-Ru(II) complexes (Fig. S2†), revealed the same trend as observed in the neutral cyclometallated series. The unsubstituted 2-pyridyl ligand (10) displayed more potent inhibition of cell survival compared to its corresponding cationic complex ([16][PF₆]₃). On the contrary, the trifluoromethyl ([17][PF₆]₃) and the methyl ([18][PF₆]₃) complexes displayed the expected enhanced cytotoxicity by 10% and 16–20%, respectively, relative to their respective ligands (11 and 12) at both tested concentrations. A comparison of the cytotoxic activity of the most active 2-pyridyl trinucleating ligands (10 and 11) and their respective complexes ([16][PF₆]₃ and [17][PF₆]₃) to that of cisplatin at 10 and 20 μM in the MCF-7 breast cancer cell line (Fig. 3) reveals interesting

trends. Firstly, the cytotoxic activity of the 5-unsubstituted 2-pyridyl ligand and complex (10 and [16][PF₆]₃, respectively) is superior to that of cisplatin at both the tested concentrations. Furthermore, the 5-trifluoromethyl complex ([17][PF₆]₃) was noted to show activity comparable to that of cisplatin at 10 and 20 μM.

As a consequence of the enhanced activity of the 2-pyridyl tris-benzimidazole ligands and related complexes in the MCF-7 breast cancer cell line, these compounds were further evaluated on the MDA-MB-231 triple-negative breast adenocarcinoma cell line. These cells represent a more aggressive, highly invasive and metastatic breast cancer subtype.⁴⁵ Cisplatin was also included as a positive control at the reported IC₅₀ value of 23 μM.⁴⁶ However, when the cytotoxic data obtained for the MDA-MB-231 cell line (Fig. S3†) were compared to that obtained for the MCF-7 cell line, the tested compounds were found to display less activity in the MDA-MB-231 cell line at 20 μM with 11 and 23% more cell viability rates than that observed in the MCF-7 cell line. An exception was [18][PF₆]₃ which was 5% more potent in the MDA-MB-231 cell line. Comparison of the cytotoxic activity of the most active ligands and complexes (10, 11, [16][PF₆]₃ and [17][PF₆]₃) to that of cisplatin at 20 μM in the MDA-MB-231 breast cancer cells reveals that all the tested compounds are less active relative to cisplatin against the MDA-MB-231 breast cancer cell line (Fig. 4).

Based on the pre-screen data summarized in Fig. 3 and 4, the 2-pyridyl ligands 10 and 11, and their corresponding trinuclear cationic complexes [16][PF₆]₃ and [17][PF₆]₃, respectively, were selected for multidose experiments, as these compounds showed the most promising activity at the fixed concentrations of 10 and 20 μM. Briefly, the MCF-7 and the MDA-MB-231 breast cancer cells were treated with a range of concentrations (5 to 35 μM) of the selected compounds for 48 h and cell viability was measured using the MTT assay. Based on the data obtained, the IC₅₀ values of the selected compounds were determined and the results are summarized in Table 2. Cisplatin was included as a positive control at the

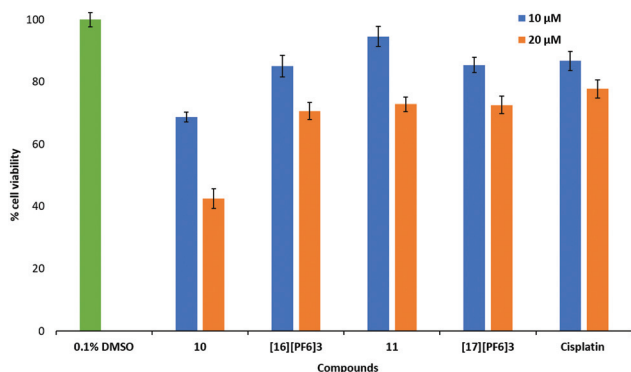


Fig. 3 The percentage cell viability as measured by MTT assays in MCF-7 breast cancer cells exposed to either vehicle (0.1% DMSO) or the most active 2-pyridyl trimeric ligands (10 and 11) and their corresponding trinuclear N^N-Ru(II) cationic complexes ([16][PF₆]₃ and [17][PF₆]₃) or cisplatin at 10 and 20 μM concentrations for 48 hours.

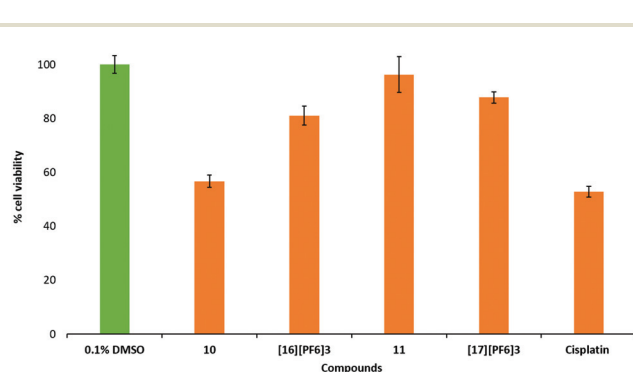


Fig. 4 The percentage cell viability as measured by MTT assays in MDA-MB-231 breast cancer cells exposed to either vehicle (0.1% DMSO) or the 2-pyridyl ligands (10 and 11) and their respective N^N-Ru(II) chelated complexes ([16][PF₆]₃ and [17][PF₆]₃) at 20 μM for 48 hours. Cisplatin (at 20 μM) was included as the positive control.

Table 2 *In vitro* anticancer activity of the selected 2-pyridyl tris-benzimidazole ligands (**10** and **11**), their corresponding trinuclear cationic complexes (**[16][PF₆]₃** and **[17][PF₆]₃**, respectively) and the mononuclear counterpart of the most active ligand and complex (**19** and **[20][PF₆]**, respectively)

Compound	5-Substituent	IC ₅₀ (μM) ± SD			Selectivity index ^c
		MCF-7	MDA-MB-231	MCF-12A	
10	H	28.65 ± 1.08	33.53 ± 1.03	38.72 ± 1.10 ^b	1.35
[16][PF₆]₃	H	33.87 ± 1.16	N/A ^a	82.42 ± 2.29 ^b	2.43
11	CF ₃	N/A ^a	N/A ^a	N/A ^a	—
[17][PF₆]₃	CF ₃	35.06 ± 1.07	N/A ^a	122.20 ± 2.62 ^b	3.49
19	H	N/A ^a	—	—	—
[20][PF₆]	H	N/A ^a	—	—	—
Cisplatin	—	35 (ref. 44)	23 (ref. 46)	36.32 ± 1.09	1.04

^a N/A: not active at tested concentrations. ^b Extrapolated by GraphPad Prism V5.01. ^c (IC₅₀ MCF-12A/IC₅₀ MCF-7).

IC₅₀ values reported in the literature of 35 μM (ref. 44) and 23 μM (ref. 46) against the MCF-7 and MDA-MB-231 cell lines, respectively. At these reported IC₅₀ values, as expected, cisplatin reduced the percentage cell survival to 50% in both the MCF-7 and MDA-MB-231 cell lines (Fig. S4 and S5†).

The 5-unsubstituted 2-pyridyl tris-benzimidazole ligand **10** and its corresponding metal complex **[16][PF₆]₃** are more active compared to cisplatin in the MCF-7 breast cancer cell line (IC₅₀ = 28.65 and 33.87 μM for **10** and **[16][PF₆]₃**, respectively, relative to IC₅₀ = 35 μM for cisplatin). The enhanced activity of **10** and **[16][PF₆]₃** relative to cisplatin in the MCF-7 cell line was also observed in the pre-screen at 10 and 20 μM (Fig. 3). The IC₅₀ value for the 5-trifluoromethyl substituted 2-pyridyl tris-benzimidazole ligand (**11**) could not be determined as the compound did not reduce MCF-7 cell survival below 50% at any of the tested concentrations (Fig. S4†). The metal complex **[17][PF₆]₃** showed comparable activity relative to cisplatin (IC₅₀ = 35.06 μM for **[17][PF₆]₃** and IC₅₀ = 35 μM for cisplatin), showing an enhancement of anticancer activity due to the presence of the ruthenium(II) centers thus highlighting the synergistic action of the metal centers and the organic ligand. The comparable cytotoxic activity of **[17][PF₆]₃** to that of cisplatin in the MCF-7 breast cancer cell line was also reflected in the pre-screen evaluation of this compound at 10 μM (Fig. 3).

When tested against the more aggressive triple-negative MDA-MB-231 cell line, the only compound that showed significant activity, albeit moderate activity, was the 2-pyridyl tris-benzimidazole **10** (IC₅₀ = 33.53 μM). Unfortunately, the IC₅₀ values of all the other selected compounds, **[16][PF₆]₃**, **11** and **[17][PF₆]₃**, could not be determined as these compounds did not inhibit MDA-MB-231 cell survival to 50% or below at any of the tested concentrations (Fig. S5†). Overall, the 5-unsubstituted ligand **10** and its corresponding cationic trimetallic complex **[16][PF₆]₃** showed the most promising activity, with either activity greater than that of clinically used cisplatin (in the MCF-7 cell line) or mild activity in the MDA-MB-231 cell line.

Cytotoxicity studies were conducted using the ligands **10** and **11** and their respective metal complexes, **[16][PF₆]₃** and

[17][PF₆]₃, to gain insight on the selectivity of the compounds towards breast cancer cells. The compounds were tested against the MCF-12A human breast epithelial cell line, where cisplatin was used as a positive control. The results attained indicate that all of the tested compounds were less cytotoxic relative to cisplatin (Table 2). The compounds **10**, **11**, and complexes **[16][PF₆]₃** and **[17][PF₆]₃** did not inhibit MCF-12A cell survival below 50% (Fig. S6 and S7†). Consequently, the IC₅₀ values for the synthesized compounds **10**, **11**, **[16][PF₆]₃** and **[17][PF₆]₃** have been extrapolated by GraphPad Prism from the data summarized in Fig. S6 and S7.† The complex **[17][PF₆]₃** has the highest selectivity, evidenced by the high IC₅₀ value (IC₅₀ = 122.20 μM) and the relatively high selectivity index (SI) value of 3.49.

By comparing the data attained for the complex **[17][PF₆]₃** to that of cisplatin (IC₅₀ = 36.53, SI = 1.04), it is evident that **[17][PF₆]₃** has activity comparable to that of cisplatin against the MCF-7 cancer cell line. However, **[17][PF₆]₃** is three times more selective towards MCF-7 breast cancer cells relative to cisplatin. Although mild cytotoxic activity is often observed in organoruthenium(II) complexes, their novel mechanisms of action as antimetastatic and antiangiogenic agents^{47,48} present a new manifold in the design of novel anticancer agents. Therefore, it may be worthwhile investigating the possible mechanisms of action of these complexes in a bid to gain a greater understanding of how these compounds exert their anticancer effects.

The mononuclear counterpart of the most active tris-benzimidazole ligand and the corresponding complex, **10** and **[16][PF₆]₃**, respectively, were also evaluated for their anticancer activity against the MCF-7 breast cancer cell line. The monomeric ligand **19** and the corresponding mononuclear cationic complex **[20][PF₆]** did not inhibit MCF-7 breast cancer cell survival to 50% or below at any of the tested concentrations (Fig. S8†). As a result, the IC₅₀ values of these compounds were not determined. In addition, a comparison of the results attained to those reported in the literature for structurally similar mononuclear and dinuclear benzimidazole-based ruthenium(II) arene complexes reveals that the trinuclear complexes investigated in this study show relatively enhanced

activity.^{22,49,50} Thus, this highlights the merit for further investigations of trinuclear systems as potential drug candidates and with a view to understanding their mechanisms of action relative to their mononuclear and dinuclear counterparts.

Conclusions

A series of novel 5-substituted 2-phenyl (7–9) and 2-pyridyl (10–12) tris-benzimidazole ligands were successfully synthesized and fully characterized. Using the synthesized tris-benzimidazole ligands 7–12, a series of corresponding cyclometallated (*C^N*)-Ru(II)-*p*-cymene (13–15) and cationic (*N^N*)-Ru(II)-*p*-cymene ([16][PF₆]₃–[18][PF₆]₃) trinuclear complexes were prepared and fully characterised. The synthesized ligands and complexes were all investigated for their antiproliferative activity at fixed concentrations of 10 and 20 μM against the MCF-7 and MDA-MB-231 breast cancer cell lines. The expected general enhancement of the anticancer activity of the compounds when tested at 20 μM compared to 10 μM was observed in MCF-7 cells. Additionally, in general, the 2-pyridyl ligands (10–12) showed slightly enhanced anticancer activity, relative to their respective 2-phenyl counterparts (7–9). The same trend was observed in the trimetallic complexes, where the cationic complexes ([16][PF₆]₃–[18][PF₆]₃) were observed to show significantly enhanced anticancer activity relative to the corresponding cyclometallated neutral analogues (13–15). From these pre-screens, 10 and 11, and their corresponding trimetallic cationic complexes [16][PF₆]₃ and [17][PF₆]₃, respectively, were selected for a further screening at various concentrations of 5–35 μM in order to determine their IC₅₀ values against the MCF-7 and MDA-MB-231 breast cancer cell lines. From the multidose screens, 10 and the corresponding complex [16][PF₆]₃ were observed to have cytotoxic activity greater than that of cisplatin against the MCF-7 cell line. The complex [17][PF₆]₃ was observed to have cytotoxicity comparable to cisplatin against the MCF-7 cell line. However, against the more aggressive MDA-MB-231 breast cancer cell line, the ligand 11, its corresponding metal complex [17][PF₆]₃ and the complex [16][PF₆]₃ were all inactive at the tested concentrations. On the contrary, 10 was observed to possess mild activity against the MDA-MB-231 cell line. In light of their promising activity, selected compounds were evaluated against the MCF-12A human breast epithelial cell line to determine selectivity. Generally, the screened compounds were observed to be less cytotoxic and more selective relative to cisplatin. Interestingly, the complex [17][PF₆]₃ was observed to have activity comparable to cisplatin against the MCF-7 breast cancer cell line and to be approximately three times more selective for MCF-7 breast cancer cells. Lastly, the mononuclear complex of the most active tris-ligand and complex, 10 and [16][PF₆]₃, respectively, were synthesized and evaluated for their anticancer activity against the MCF-7 breast cancer cell line. Both the monomeric ligand and the corresponding cationic complex, 19 and [20][PF₆]₃, did not inhibit

MCF-7 breast cancer survival to 50% or below at the tested concentrations. This further highlights the merit in investigating multimeric benzimidazole-based ligands, and also the advantage of having more than one Ru(II) center. These promising results contribute to the growing interest in multinuclear organoruthenium(II) compounds as potential anticancer agents, as these compounds are known to show antitumour activity and other novel mechanisms of action. Further investigations into the possible mechanisms of action of these promising compounds in this study are ongoing.

Experimental

Materials

All reactions were carried out in an inert argon atmosphere, unless stated otherwise. All reagents were purchased from commercial sources (Sigma-Aldrich, Combi-blocks) and used without further purification. The [Ru(*p*-cymene)Cl₂]₂ dimeric precursor was prepared following a literature method.⁵¹ The ligand precursors *N*¹-(2-nitrophenyl)-*N*²,*N*²-bis(2-((2-nitrophenyl)amino)ethyl)ethane-1,2-diamine and *N*¹-(2-(bis(2-((2-aminophenyl)amino)ethyl)amino)ethyl)benzene-1,2-diamine⁵² were synthesized following adapted literature methods.

Equipment and instrumentation

Reactions were monitored by TLC using aluminium-backed Merck silica-gel F254 plates, and compounds were visualised under UV-lamp. All column chromatography was carried out using Fluka Silica Gel 60, 40–63 microns. Nuclear Magnetic Resonance spectra were recorded on either a Bruker X400 MHz spectrometer (¹H at 399.95 MHz and ¹³C at 100.65 MHz) or a Varian Mercury XR300 MHz (¹H at 299.95 MHz, ¹³C at 75.46 MHz) with tetramethylsilane (TMS) as the internal standard for chemical shifts. Chemical shifts and *J*-coupling values were reported in ppm and Hz, respectively. Infrared spectroscopy was conducted on a Perkin-Elmer Spectrum 100 FT-IR spectrometer using Attenuated Total Reflectance (ATR) with bond vibrations measured in reciprocal centimetres (cm⁻¹). Mass spectrometry (MS) determinations were carried out using Electron Impact (EI) on JEOL GCmatell instrument or Electrospray Ionisation (ESI) on a Waters API Quattro Micro triple quadrupole mass spectrometer with data recorded using the positive mode. A Büchi Melting Point Apparatus B-540 machine was used to obtain the uncorrected melting points of each compound. Determination of C/H/N was done using a 2400 CHN elemental analyzer by Perkin Elmer.

The general procedure for the synthesis of tris-nitrobenzene precursors (1–3)

Tris(2-aminoethyl)amine (1 eq.) was dissolved in DMF (5 mL) at room temperature, under argon atmosphere. Thereafter, the appropriate nitrobenzene (3 eq.) was added to the reaction vessel and the reaction was allowed to stir at room temperature for 24 h under argon, reaction progress was monitored by TLC analysis. Upon completion, the reaction mixture was

diluted with a saturated brine solution (30 mL) and the extracted with two aliquots of ethyl acetate (2 × 30 mL). The organic extracts were combined and dried over anhydrous sodium sulfate, and excess solvent was removed *in vacuo*. The resultant crude product was purified using column chromatography to afford the desired tris-nitrobenzene product.

***N*¹-(2-Nitrophenyl)-*N*²,*N*²-bis(2-((2-nitrophenyl)amino)ethyl)ethane-1,2-diamine (1).**⁵² Tris(2-aminoethyl)amine (0.500 mL, 3.34 mmol) was reacted with 1-fluoro-2-nitrobenzene (1.06 mL, 10.1 mmol) at room temperature for 24 h, under argon. The desired compound (1) was isolated as a bright yellow solid (1.11 g, 2.18 mmol). *R*_f (4 : 6 ethyl acetate : petroleum ether): 0.50. **Yield:** 48.3%. ¹H NMR (300 MHz, DMSO) δ (ppm): 8.21 (t, ³*J*_{HH} = 5.1 Hz, 3H, NH), 8.00 (dd, ³*J*_{HH} = 8.6 Hz, ⁴*J*_{HH} = 1.6 Hz, 3H, ArH), 7.46 (ddd, ²*J*_{HH} = 8.5 Hz, ³*J*_{HH} = 7.0 Hz, ⁴*J*_{HH} = 1.4 Hz, 3H, ArH), 6.98 (d, ³*J*_{HH} = 8.0 Hz, 3H, ArH), 6.64 (ddd, ²*J*_{HH} = 8.3 Hz, ³*J*_{HH} = 6.9, ⁴*J*_{HH} = 1.1 Hz, 3H, ArH), 3.45 (q, *J* = 6.1 Hz, 6H, CH₂), 2.90 (t, ³*J*_{HH} = 6.3 Hz, 6H, CH₂). ¹³C{¹H}-NMR (101 MHz, DMSO) δ (ppm): 145.50, 136.87, 131.53, 126.64, 115.55, 114.85, 52.93, 41.19. **MP** (°C): 103.8–105.3.

***N*¹-(2-Nitro-4-(trifluoromethyl)phenyl)-*N*²,*N*²-bis(2-((2-nitro-4-(trifluoromethyl)phenyl)amino)ethyl)ethane-1,2-diamine (2).** Tris(2-aminoethyl)amine (0.500 mL, 3.34 mmol) and 4-chloro-3-nitrobenzotrifluoride (1.49 mL, 10.0 mmol) were dissolved in DMF and allowed to stir at room temperature for 24 h, under argon. The pure compound (2) was isolated as a bright yellow solid (0.841 g, 1.18 mmol). *R*_f (2 : 1 petroleum ether : ethyl acetate): 0.56. **Yield:** 35.3%. ¹H NMR (300 MHz, DMSO) δ (ppm): 8.45 (t, ³*J*_{HH} = 5.0 Hz, 3H, NH), 8.15 (d, ³*J*_{HH} = 1.6 Hz, 3H, ArH), 7.66 (dd, ³*J*_{HH} = 9.1, ⁴*J*_{HH} = 2.1 Hz, 3H, ArH), 7.15 (d, ³*J*_{HH} = 9.1 Hz, 3H, ArH), 3.49 (dd, ³*J*_{HH} = 11.0, ⁴*J*_{HH} = 5.5 Hz, 6H, CH₂), 2.92 (t, ³*J*_{HH} = 5.9 Hz, 6H, CH₂). ¹³C{¹H}-NMR (101 MHz, DMSO) δ (ppm): 146.49, 131.53, 129.96, 124.97, 123.68, 115.60, 114.70, 52.17, 40.80. **MP** (°C): 170.6–172.1.

***N*¹-(4-Methyl-2-nitrophenyl)-*N*²,*N*²-bis(2-((4-methyl-2-nitrophenyl)amino)ethyl)ethane-1,2-diamine (3).** Tris(2-aminoethyl)amine (0.500 mL, 3.34 mmol) and 4-fluoro-2-nitrotoluene (1.55 g, 10.0 mmol) were dissolved in DMF and allowed to stir at room temperature for 24 h, under argon. The pure compound (3) was isolated as a dark orange solid (0.887 g, 1.62 mmol). *R*_f (4 : 1 petroleum ether : ethyl acetate): 0.51. **Yield:** 39.2%. ¹H NMR (300 MHz, DMSO) δ (ppm): 8.08 (t, ³*J*_{HH} = 5.0 Hz, 3H, NH), 7.79 (d, ³*J*_{HH} = 1.0 Hz, 3H, ArH), 7.29 (dd, ³*J*_{HH} = 8.8 Hz, ⁴*J*_{HH} = 1.9 Hz, 3H, ArH), 6.89 (d, ³*J*_{HH} = 8.8 Hz, 3H, ArH), 3.41 (dd, ³*J*_{HH} = 11.5 Hz, ⁴*J*_{HH} = 5.9 Hz, 6H, CH₂), 2.87 (t, ³*J*_{HH} = 6.2 Hz, 6H, CH₂), 2.20 (s, 9H, CH₃). ¹³C{¹H}-NMR (101 MHz, DMSO) δ (ppm): 143.33, 137.76, 130.53, 125.07, 124.02, 114.39, 52.47, 40.7, 19.36. **MP** (°C): 125.6–127.3.

General synthesis of tris-1,2-benzenediamines (4–6)

The appropriate tris-nitrobenzene (1 eq.) was dissolved in dry methanol (10 mL), under argon and allowed to stir for 5 minutes. Ammonium chloride (30 eq.) and zinc (60 eq.) were added to the reaction vessel, under argon. The reaction vessel was allowed to stir at room temperature for 1 h, under

argon. After 1 hour, TLC analysis showed a complete conversion of the limiting reagent to a new product. The reaction mixture was filtered through Celite® and rinsed with copious methanol. The filtrate was subsequently collected, and the excess solvent was reduced by rotary evaporation. The resultant residue was re-dissolved in ethyl acetate (30 mL) and washed with two aliquots of a saturated sodium bicarbonate solution (2 × 30 mL), a 1 M solution of sodium hydroxide (30 mL) and deionized water (30 mL). The organic extract was collected, dried over anhydrous sodium sulfate and excess solvent was reduced *in vacuo* and the resultant crude was purified using column chromatography (100% ethyl acetate).

***N*¹-(2-(Bis(2-((2-aminophenyl)amino)ethyl)amino)ethyl)benzene-1,2-diamine (4).**⁵² *N*¹-(2-Nitrophenyl)-*N*²,*N*²-bis(2-((2-nitrophenyl)amino)ethyl)ethane-1,2-diamine (0.810 g, 1.59 mmol) was reacted with ammonium chloride (2.52 g, 47.0 mmol) and zinc powder (6.16 g, 94.2 mmol) at room temperature for 24 h. The desired product (4) was isolated as a dark brown solid (0.778 g, 1.86 mmol). *R*_f (ethyl acetate): 0.45. **Yield:** 97.0%. ¹H NMR (300 MHz, DMSO) δ (ppm): 6.57 (dd, ³*J*_{HH} = 7.2 Hz, ⁴*J*_{HH} = 1.5 Hz, 3H, ArH), 6.53–6.38 (m, 9H, ArH), 4.38 (s, 9H, NH and NH₂), 3.13 (dd, ³*J*_{HH} = 4.7 Hz, ⁴*J*_{HH} = 11.8 Hz, 6H, CH₂), 2.79 (t, ³*J*_{HH} = 6.6 Hz, 6H, CH₂). ¹³C{¹H}-NMR (101 MHz, DMSO) δ (ppm): 136.77, 135.75, 118.42, 117.48, 114.98, 110.67, 53.61, 42.18. **FT-IR** (ATR) ν (cm⁻¹): 3366 and 3299 (1° amine). **MP** (°C): 121.7–123.8.

***N*¹-(2-(Bis(2-((2-amino-4-(trifluoromethyl)phenyl)amino)ethyl)amino)ethyl)-4-(trifluoromethyl)benzene-1,2-diamine (5).** *N*¹-(2-Nitro-4-(trifluoromethyl)phenyl)-*N*²,*N*²-bis(2-((2-nitro-4-(trifluoromethyl)phenyl)amino)ethyl)ethane-1,2-diamine (0.603 g, 0.842 mmol), ammonium chloride (1.35 g, 25.2 mmol) and zinc powder (3.32 g, 50.8 mmol) were reacted in anhydrous methanol at room temperature for 1 h, under argon. The product (5) was isolated as a beige solid (0.660 g, 0.706 mmol). *R*_f (1 : 1 ethyl acetate : petroleum ether): 0.97. **Yield:** 83.8%. ¹H NMR (300 MHz, DMSO) δ (ppm): 6.83 (d, ³*J*_{HH} = 2.0 Hz, 3H, ArH), 6.74 (d, ³*J*_{HH} = 8.3 Hz, 3H, ArH), 6.45 (d, ³*J*_{HH} = 8.2 Hz, 3H, ArH), 5.02 (t, ³*J*_{HH} = 5.2 Hz, 3H, NH), 4.84 (s, 6H, NH₂), 3.19 (dd, ³*J*_{HH} = 11.9 Hz, ⁴*J*_{HH} = 6.0 Hz, 6H, CH₂), 2.78 (t, ³*J*_{HH} = 6.6 Hz, 6H, CH₂). ¹³C{¹H}-NMR (101 MHz, DMSO) δ (ppm): 139.03, 135.08, 124.07, 116.46 (q, ⁴*J*_{C-F} = 31.0 Hz), 114.70, 109.69, 108.28, 52.63, 41.35. **FT-IR** (ATR) ν (cm⁻¹): 3342 and 3306 (1° amine). **MP** (°C): 183.9–185.6.

***N*¹-(2-(Bis(2-((2-amino-4-methylphenyl)amino)ethyl)amino)ethyl)-4-methylbenzene-1,2-diamine (6).** *N*¹-(4-Methyl-2-nitrophenyl)-*N*²,*N*²-bis(2-((4-methyl-2-nitrophenyl)amino)ethyl)ethane-1,2-diamine (1.11 g, 2.01 mmol) was reacted with ammonium chloride (3.17 g, 59.3 mmol) and zinc powder (6.76 g, 103 mmol) in anhydrous methanol, under argon for 1 h. The desired product (6) was isolated as a brown solid (0.668 g, 1.45 mmol). *R*_f (ethyl acetate): 0.14. **Yield:** 75.1%. ¹H NMR (300 MHz, DMSO) δ (ppm): 6.40 (d, ³*J*_{HH} = 1.1 Hz, 3H, ArH), 6.32 (m, 6H, H-e, ArH), 4.32 (s, 6H, NH₂), 4.25 (t, ³*J*_{HH} = 5.0 Hz, 3H, NH), 3.07 (d, ³*J*_{HH} = 4.8 Hz, 6H, CH₂), 2.74 (t, ³*J*_{HH} = 6.4 Hz, 6H, CH₂), 2.08 (s, 9H, CH₃). ¹³C{¹H}-NMR (101 MHz, DMSO) δ (ppm): 135.96, 134.42, 125.99, 118.60, 115.90, 111.12, 53.70,

42.47, 20.91. **FT-IR** (ATR) ν (cm⁻¹): 3318 and 3373 (1° amine). **MP** (°C): 128.3–130.2.

General synthetic procedure for the tris-benzimidazole ligands (7–12)

The appropriate tris-1,2-benzenediamine (4–6) (1 eq.) was dissolved in dry ethanol (6 mL), and allowed to stir under argon for 5 minutes. Benzaldehyde or 2-pyridinecarboxaldehyde (3.6 eq.) was added to the reaction vessel, under argon. Thereafter, magnesium sulfate (18 eq.) and trifluoroacetic acid (0.3 eq.) were added to the reaction vessel, under argon. The reaction mixtures with benzaldehyde were refluxed at 80 °C for 24 h and the reactions with 2-pyridinecarboxaldehyde were stirred at room temperature for 24 h, open to air. TLC analysis confirmed the successful conversion of starting materials to a new product. The reaction mixture was subsequently filtered and the filtrate collected. The excess solvent was removed by rotary evaporation, and the resultant crude was re-dissolved in ethyl acetate (30 mL) and washed with a saturated sodium bicarbonate solution (30 mL) and a saturated brine solution (30 mL). The organic extract was collected and dried over anhydrous sodium sulfate, and the excess solvent was removed *in vacuo*. The resultant residue was purified using column chromatography.

Tris(2-(2-phenyl-1H-benzo[d]imidazol-1-yl)ethyl)amine (7). Pale yellow solid (7) (0.0740g, 0.109 mmol). *R_f* (7 : 3 ethyl acetate : petroleum ether): 0.21. **Yield**: 51.1%. **¹H NMR** (400 MHz, DMSO) δ (ppm): 7.68–7.62 (m, 3H, ArH), 7.59–7.53 (m, 6H, ArH), 7.48–7.40 (m, 9H, ArH), 7.29–7.22 (m, 6H, ArH), 7.20–7.15 (m, 3H, ArH), 3.79 (t, ³*J*_{HH} = 7.1 Hz, 6H, CH₂), 2.41 (t, ³*J*_{HH} = 7.1 Hz, 6H, CH₂). **¹³C{¹H}-NMR** (101 MHz, DMSO) δ (ppm): 153.59, 143.0, 135.71, 130.81, 130.08, 129.43, 129.13, 123.00, 122.52, 119.70, 110.91, 52.91, 42.75. **FT-IR** (ATR) ν (cm⁻¹): 1695 (imine C=N). **MP** (°C): 193.6–196.2. **Purity** 98% by LC (*t_R* 2.823 min).

Tris(2-(2-phenyl-5-(trifluoromethyl)-1H-benzo[d]imidazol-1-yl)ethyl)amine (8). Cream solid (8) (0.0952 g, 0.108 mmol). *R_f* (1 : 1 ethyl acetate : petroleum ether): 0.18. **Yield**: 70.3%. **¹H NMR** (300 MHz, DMSO) δ (ppm): 8.01 (s, 3H, ArH), 7.61–7.54 (m, 6H, ArH), 7.52 (dd, ³*J*_{HH} = 8.7 Hz, ⁴*J*_{HH} = 1.4 Hz, 3H, ArH), 7.48–7.39 (m, 12H, ArH), 3.88 (t, ³*J*_{HH} = 6.6 Hz, 6H, CH₂), 2.36 (t, *J* = 6.6 Hz, 6H, CH₂). **¹³C{¹H}-NMR** (101 MHz, DMSO) δ (ppm): 155.87, 142.41, 138.00, 130.51, 130.11, 129.49, 129.21, 126.78, 123.55 (q, ⁴*J*_{C-F} = 35.9 Hz), 119.47, 117.06, 112.01, 52.43, 42.88. **FT-IR** (ATR) ν (cm⁻¹): 1626 (imine C=N). **MP** (°C): 204.4–205.1. **Purity** 94% by LC (*t_R* 2.880 min).

Tris(2-(5-methyl-2-phenyl-1H-benzo[d]imidazol-1-yl)ethyl)amine (9). White solid (9) (0.0723 g, 0.100 mmol). *R_f* (1 : 1 petroleum ether : ethyl acetate): 0.12. **Yield**: 46.4%. **¹H NMR** (300 MHz, CDCl₃) δ (ppm): 7.58 (s, 3H, ArH), 7.55–7.48 (m, 6H, ArH), 7.44–7.35 (m, 9H, H-m, ArH), 7.07 (dd, ³*J*_{HH} = 8.2 Hz, ⁴*J*_{HH} = 1.1 Hz, 3H, ArH), 6.78 (d, ³*J*_{HH} = 8.2 Hz, 3H, ArH), 3.69 (t, ³*J*_{HH} = 7.0 Hz, 6H, CH₂), 2.50 (s, 9H, CH₃), 2.37 (t, ³*J*_{HH} = 7.0 Hz, 6H, CH₂). **¹³C{¹H}-NMR** (101 MHz, CDCl₃) δ (ppm): 153.41, 143.07, 133.17, 132.53, 130.37, 129.92, 129.07, 128.83, 124.55, 119.94, 109.07, 53.43, 42.78, 21.56. **FT-IR** (ATR) ν (cm⁻¹): 1625

(imine C=N). **MP** (°C): 197.6–199.8. **Purity** 97% by LC (*t_R* 2.703 min).

Tris(2-(2-(pyridin-2-yl)-1H-benzo[d]imidazol-1-yl)ethyl)amine (10). Pale brown solid (10) (0.0300g, 0.0441 mmol). *R_f* (7 : 3 ethyl acetate : petroleum ether): 0.22. **Yield**: 34.8%. **¹H NMR** (300 MHz, DMSO) δ (ppm): 8.30 (m, 6H, ArH), 7.92 (td, ³*J*_{HH} = 7.8 Hz, ⁴*J*_{HH} = 1.5 Hz, 3H, ArH), 7.76–7.69 (m, 3H, ArH), 7.41–7.23 (m, 12H, ArH), 4.60 (t, ³*J*_{HH} = 6.8 Hz, 6H, CH₂), 2.97 (t, ³*J*_{HH} = 6.9 Hz, 6H, CH₂). **¹³C{¹H}-NMR** (101 MHz, DMSO) δ (ppm): 149.81, 149.37, 148.39, 142.04, 137.26, 136.22, 124.17, 124.02, 123.13, 122.32, 119.53, 110.42, 53.64, 43.38. **FT-IR** (ATR) ν (cm⁻¹): 1733 (imine C=N), 1586 (pyridyl C=N). **MP** (°C): 183.5–184.9. **Purity** 99% by LC (*t_R* 2.816 min).

Tris(2-(2-(pyridin-2-yl)-5-(trifluoromethyl)-1H-benzo[d]imidazol-1-yl)ethyl)amine (11). Cream white solid (11) (0.0203 g, 0.0229 mmol). *R_f* (2 : 1 petroleum ether : ethyl acetate): 0.13. **Yield**: 40.3%. **¹H NMR** (300 MHz, DMSO) δ (ppm): 8.35 (d, *J* = 4.2 Hz, 3H, ArH), 8.29 (d, ³*J*_{HH} = 7.9 Hz, 3H, ArH), 8.10 (s, 3H, ArH), 7.95 (t, ³*J*_{HH} = 7.4 Hz, 3H, ArH), 7.66–7.53 (m, 6H, H-g, ArH), 7.42–7.33 (m, 3H, ArH), 4.65 (t, ³*J*_{HH} = 6.5 Hz, 6H, CH₂), 3.03 (t, ³*J*_{HH} = 6.3 Hz, 6H, CH₂). **¹³C{¹H}-NMR** (151 MHz, DMSO) δ (ppm): 152.29, 149.76, 149.06, 142.03, 139.03, 137.96, 125.12, 125.06, 124.10, 120.03, 117.48, 112.14, 60.06, 53.86, 44.28. **FT-IR** (ATR) ν (cm⁻¹): 1620 (imine C=N), 1587 (pyridyl C=N). **MP** (°C): 201.3–202.0. **Purity** 94% by LC (*t_R* 3.038 min).

Tris(2-(5-methyl-2-(pyridin-2-yl)-1H-benzo[d]imidazol-1-yl)ethyl)amine (12). Cream solid (12) (0.0530 g, 0.0733 mmol). *R_f* (7 : 3 ethyl acetate : petroleum ether): 0.27. **Yield**: 33.8%. **¹H NMR** (400 MHz, CDCl₃) δ (ppm): 8.41 (d, ³*J*_{HH} = 8.0 Hz, 3H, ArH), 8.30 (d, ³*J*_{HH} = 4.5 Hz, 3H, ArH), 7.77 (td, ³*J*_{HH} = 7.8 Hz, ⁴*J*_{HH} = 1.8 Hz, 3H, ArH), 7.63 (s, 3H, ArH), 7.22–7.06 (m, 9H, ArH), 4.81–4.74 (m, 6H, CH₂), 3.27–3.14 (m, 6H, CH₂), 2.51 (s, 9H, CH₃). **¹³C{¹H}-NMR** (101 MHz, CDCl₃) δ (ppm): 150.50, 149.65, 148.52, 142.86, 136.77, 134.75, 132.54, 125.17, 124.57, 123.62, 119.91, 109.4, 54.66, 44.38, 21.60. **FT-IR** (ATR) ν (cm⁻¹): 1726 (imine C=N), 1590 (pyridyl imine C=N). **MP** (°C): 170.1–173.5. **Purity** 99% by LC (*t_R* 2.969 min).

Cyclometallated Ru(II)-*p*-cymene metal complex (13). Tris(2-(2-phenyl-1H-benzo[d]imidazol-1-yl)ethyl)amine (0.0353g, 0.0516 mmol) was dissolved in 1 : 1 DCM : ethanol (30 mL) under argon. To this brown solution, dichloro(*p*-cymene)ruthenium(II) dimer (0.0474 g, 0.0774 mmol), sodium acetate (0.00853 g, 0.103 mmol) was added and the mixture was allowed to stir at room temperature for 24 h, under argon. After TLC analysis confirmed the conversion of the limiting reagent to a product spot, the reaction mixture was filtered through Celite®. The filtrate was collected, and excess solvent was reduced to *ca.* 1 mL, and this crude mixture was subjected to trituration in chloroform for 24 h. A dark green crude was isolated by suction filtration, and this was re-dissolved in DCM (1 mL) and precipitated in pentane. The desired product (13) was isolated as a light green powder (0.0704 g, 0.0473 mmol) by suction filtration. **Yield**: 84.9%. **¹H NMR** (300 MHz, DMSO) δ (ppm): 8.27 (d, ³*J*_{HH} = 7.3 Hz, 3H, ArH), 7.97 (d, ³*J*_{HH} = 8.0 Hz, 3H, ArH), 7.60–7.12 (m, 12H, ArH), 7.06

(t, $^3J_{\text{HH}} = 7.4$ Hz, 3H, ArH), 6.86 (m, 3H, ArH), 5.97 (dd, $^3J_{\text{HH}} = 13.7$ Hz, $^4J_{\text{HH}} = 6.9$ Hz, 3H, Ar_{p-cye}), 5.75–5.63 (m, 3H, Ar_{p-cye}), 5.37 (dt, $^3J_{\text{HH}} = 11.2$, 5.7 Hz, 3H, Ar_{p-cye}), 5.19 (t, $^3J_{\text{HH}} = 5.8$ Hz, 3H, Ar_{p-cye}), 4.42 (s, 6H, CH₂), 2.92 (bs, 6H, CH₂), 1.63 (s, 9H, CH₃ p-cye), 0.70–0.54 (m, 9H, CH(CH₃)₂ p-cye), 0.53–0.36 (m, 9H, CH(CH₃)₂ p-cye). $^{13}\text{C}\{^1\text{H}\}$ -NMR (101 MHz, DMSO) δ (ppm): 141.34, 124.11, 123.63, 122.54, 117.91, 111.05, 89.75, 89.88, 82.56, 81.06, 53.93, 43.59, 30.69, 22.42, 21.70, 18.84. FT-IR (ATR) ν (cm⁻¹): 1580 (imine C=N). MP (°C): 275.1 (decomp.). MS (HR-ESI, *m/z*): Calculated: 1488.2580, Found: 1488.2526 (100%, [M + H]⁺).

Trifluoromethyl substituted Ru(II) cyclometallated complex (14). Tris(2-(2-phenyl-5-(trifluoromethyl)-1H-benzo[d]imidazol-1-yl)ethyl)amine (0.0210 g, 0.0227 mmol) was dissolved in anhydrous acetonitrile (10 mL), under argon. The dichloro(*p*-cymene)ruthenium(II) dimer (0.0222 g, 0.0363 mmol) and sodium acetate (0.0112 g, 0.136 mmol) were then added to the reaction vessel, under argon. The reaction mixture was then allowed to stir at room temperature for 24 h, after which the complete reaction of the limiting reagent was observed upon TLC analysis. The reaction mixture was then filtered through Celite® and the filtrate was collected. Excess solvent was removed by rotary evaporation and the resulting crude was re-dissolved in DCM (*ca.* 1 mL). Hexane was subsequently added to the vessel, resulting in a dark yellow precipitate (14) which was isolated by suction filtration (0.0479 g, 0.0283 mmol). Yield: 83.3%. ^1H NMR (300 MHz, CDCl₃) δ (ppm): 8.30 (d, $^3J_{\text{HH}} = 7.5$ Hz, 3H, ArH), 7.99 (m, 3H, ArH), 7.59–7.23 (m, 15H, ArH), 6.99–6.69 (m, 6H, ArH), 5.77 (t, $^3J_{\text{HH}} = 5.7$ Hz, 3H, Ar_{p-cye}), 5.66 (t, $^3J_{\text{HH}} = 5.4$ Hz, 3H, Ar_{p-cye}), 5.36–5.16 (m, 3H, Ar_{p-cye}), 5.02 (t, $^3J_{\text{HH}} = 5.3$ Hz, 3H, Ar_{p-cye}), 3.67 (bs, 6H, CH₂), 2.33–2.08 (m, 9H, CH₂, CH(CH₃)₂ p-cye), 1.98 (dd, $^3J_{\text{HH}} = 5.4$ Hz, $^4J_{\text{HH}} = 2.4$ Hz, 9H, CH₃ p-cye), 0.80 (dd, $^3J_{\text{HH}} = 13.8$ Hz, $^4J_{\text{HH}} = 8.4$ Hz, 9H, CH(CH₃)₂ p-cye), 0.64 (dd, $^3J_{\text{HH}} = 12.6$ Hz, $^4J_{\text{HH}} = 6.0$ Hz, 9H, CH(CH₃)₂ p-cye). $^{13}\text{C}\{^1\text{H}\}$ -NMR (151 MHz, CDCl₃) δ (ppm): 161.05, 142.17, 138.99, 135.47–133.80 (m), 131.85, 130.41, 126.40, 123.88, 121.63, 116.83–114.65 (m), 113.66, 103.81–103.05 (m), 101.64–100.21 (m), 91.49, 90.30, 83.33, 81.98, 53.39, 45.73 (d, $J = 37.0$ Hz), 44.24, 32.30, 31.09, 23.86, 23.17, 20.37, 15.50. FT-IR (ATR) ν (cm⁻¹): 1581 (imine C=N). MS (HR-ESI, *m/z*): Calculated: 1156.9920, Found: 1157.3227 (40% [M + Na - C₂₆H₂₅ClF₃N₂Ru]⁺). Elemental analysis for C₇₈H₇₅Cl₃F₉N₇Ru₃·3H₂O (1745.098 g mol⁻¹): Found (%) C, 53.95%; H, 4.31%; N, 6.12%; Calculated (%) C, 53.69%; H, 4.68%; N, 5.62%.

Methyl substituted Ru(II) cyclometallated complex (15). Tris(2-(5-methyl-2-phenyl-1H-benzo[d]imidazol-1-yl)ethyl)amine (0.0291 g, 0.0405 mmol) was dissolved in anhydrous acetonitrile (8 mL) under argon. To this transparent solution, dichloro(*p*-cymene)ruthenium(II) dimer (0.0384 g, 0.0627 mmol), sodium acetate (0.0350 g, 0.427 mmol) was added and the mixture was allowed to stir at room temperature for 24 h, under argon. After TLC analysis (in ethyl acetate) confirmed the complete conversion of the limiting reagent to a product spot, the reaction mixture was filtered through Celite®. The filtrate was collected and excess solvent was

removed and the resultant crude was re-dissolved in *ca.* 1 mL DCM and hexane (12 mL) was subsequently added to the solution. This resulted in the precipitation of a dark yellow-brownish precipitate (15) which was isolated *via* suction filtration (0.0638 g, 0.0417 mmol). Yield: 88.3%. ^1H NMR (300 MHz, DMSO) δ (ppm): 8.26 (t, $^3J_{\text{HH}} = 6.7$ Hz, 3H, ArH), 7.72 (d, $^3J_{\text{HH}} = 4.4$ Hz, 3H, ArH), 7.61–6.73 (m, 18H, ArH), 6.11–5.88 (m, 3H, Ar_{p-cye}), 5.68 (t, $^3J_{\text{HH}} = 6.0$ Hz, 3H, Ar_{p-cye}), 5.47–5.27 (m, 3H, Ar_{p-cye}), 5.23–5.12 (m, 3H, Ar_{p-cye}), 4.54–4.23 (m, 6H, CH₂), 2.84–2.74 (m, 6H, CH₂), 2.65–2.55 (m, 6H, Ar-CH₃), 2.42 (d, $^3J_{\text{HH}} = 3.9$ Hz, 3H, CH₃), 1.95–1.62 (m, 12H, CH₃ p-cye, CH(CH₃)₂ p-cye), 0.72–0.54 (m, 9H, CH(CH₃)₂ p-cye), 0.51–0.35 (m, 9H, CH(CH₃)₂ p-cye). $^{13}\text{C}\{^1\text{H}\}$ -NMR (151 MHz, DMSO) δ (ppm): 157.46, 146.16, 145.41, 141.62, 141.32, 135.00, 134.15, 134.05, 133.00, 129.25, 128.10, 126.53, 124.91, 123.93, 122.46, 89.88, 88.88, 82.93, 80.84, 33.43, 30.78, 24.43, 22.38, 21.79, 21.01, 18.94. MS (HR-ESI, *m/z*): Calculated: 1494.0329, Found: 1494.3296 (70% [M - Cl]⁺). Elemental analysis for C₇₈H₈₄Cl₃N₇Ru₃·3H₂O (1583.184 g mol⁻¹): Found (%) C, 59.36%; H, 5.82%; N, 5.85%; Calculated (%) C, 59.18%; H, 5.73%; N, 6.19%.

General synthetic procedure for the cationic *N,N*-Ru(II)-*p*-cymene metal complexes ([16][PF₆]₃–[18][PF₆]₃)

The ruthenium dimer [Ru(η⁶-*p*-Pr¹C₆H₄Me)Cl₂]₂ (1.5 eq.) was added to a stirring solution of the appropriate 2-pyridyl tris-benzimidazole ligand (1 eq.) in a 1:1 solution of DCM:ethanol, under argon. The reaction mixture was allowed to stir at room temperature for 24 h, under argon. After TLC analysis confirmed the complete reaction of the limiting reagent, the contents of the reaction flask were filtered through Celite® and the filtrate was collected. NH₄PF₆ (4 eq.) was added to the filtrate and was allowed to stir for at room temperature for 1 h, under argon. The DCM was removed from the reaction mixture under reduced pressure, which resulted in the precipitation of a yellow solid. The solid was isolated by suction filtration, washed with cold ethanol and dried.

Cationic *N,N*-Ru(II)-*p*-cymene metal complex ([16][PF₆]₃). Tris(2-(2-phenyl-1H-benzo[d]imidazol-1-yl)ethyl)amine (0.0354 g, 0.0520 mmol) was reacted with dichloro(*p*-cymene)ruthenium(II) dimer (0.0478 g, 0.0780 mmol) at room temperature for 24 h. NH₄PF₆ (0.0487 g, 0.299 mmol) was added to crude and stirred for 1 h. The desired product ([16][PF₆]₃) was isolated by vacuum filtration as a dark yellow solid (0.0435 g, 0.0265 mmol). Yield: 51.1%. ^1H NMR (300 MHz, DMSO) δ (ppm): 9.69–9.55 (m, 3H, ArH), 8.14–7.92 (m, 9H, ArH), 7.83–7.40 (m, 12H, ArH), 6.31 (d, $^3J_{\text{HH}} = 6.0$ Hz, 3H, Ar_{p-cye}), 6.27 (d, $^3J_{\text{HH}} = 6.0$ Hz, 3H, Ar_{p-cye}), 6.13 (d, $^3J_{\text{HH}} = 5.1$ Hz, 3H, Ar_{p-cye}), 6.05 (d, $^3J_{\text{HH}} = 5.8$ Hz, 3H, Ar_{p-cye}), 4.60–4.23 (m, 6H, CH₂), 3.11–2.80 (m, 6H, CH₂), 2.42–2.24 (m, 3H, CH(CH₃)₂ p-cye), 2.13 (s, 9H, CH₃ p-cye), 0.91–0.73 (m, 9H, CH(CH₃)₂ p-cye). $^{13}\text{C}\{^1\text{H}\}$ -NMR (101 MHz, DMSO) δ (ppm): 157.98, 148.39, 145.46, 140.23, 127.64, 126.90, 126.18, 124.69, 119.46, 119.31, 119.19, 112.94, 84.53, 83.16, 80.72, 79.64, 52.32, 44.36, 30.96, 22.25, 22.13, 19.09. $^{31}\text{P}\{^1\text{H}\}$ -NMR (162 MHz, DMSO) δ (ppm):

–144.13 (sep, $J = 711.2$ Hz, PF₆). **FT-IR** (ATR) ν (cm⁻¹): 1599 (imine C=N), 1481 (pyridyl C=N). **MP** (°C): 225.2 (decomp.). **MS (HR-ESI, m/z)**: Calculated: 1782.9679, Found: 1783.0917 (40%, [M – PF₆]⁺).

Trifluoromethyl substituted cationic *N,N*-Ru(II)-*p*-cymene metal complex ([17][PF₆]₃). The ruthenium dimer [Ru(η^6 -*p*-PrⁱC₆H₄Me)Cl₂]₂ (0.0636 g, 0.104 mmol) was reacted with tris (2-(2-(pyridin-2-yl)-5-(trifluoromethyl)-1*H*-benzo[*d*]imidazol-1-yl)ethyl)amine (0.0529 g, 0.0735 mmol) at room temperature. NH₄PF₆ (0.0356 g, 0.434 mmol) was added to the filtrate and stirred for 1 h. The desired product ([17][PF₆]₃) was isolated as a bright yellow solid (0.0523 g, 0.0293 mmol). **Yield**: 69.3%. **¹H NMR (600 MHz, DMSO) δ (ppm)**: 9.68–9.60 (m, 3H, ArH), 8.17–7.99 (m, 9H, ArH), 7.94–7.83 (m, 6H, ArH), 7.82–7.70 (m, 3H, ArH), 6.37–6.26 (m, 6H, Ar-*p*-cye), 6.13 (dd, ³J_{HH} = 13.1 Hz, ⁴J_{HH} = 6.5 Hz, 3H, Ar-*p*-cye), 6.07–5.99 (m, 3H, Ar-*p*-cye), 4.68–4.32 (m, 6H, CH₂), 3.12–2.89 (m, 6H, CH₂), 2.47–2.40 (m, 3H, CH(CH₃)₂ *p*-cye), 2.13–2.08 (m, 9H, CH₃ *p*-cye), 0.91–0.83 (m, 18H, CH(CH₃)₂ *p*-cye). **¹³C{¹H}-NMR (151 MHz, DMSO) δ (ppm)**: 158.13, 150.88, 144.84, 140.91, 139.88, 138.47, 128.22, 125.76, 123.38, 116.14, 115.05, 104.51, 87.20, 84.96, 83.41, 81.69, 52.48, 45.20, 31.46, 22.31, 22.16, 19.34. **³¹P{¹H}-NMR (162 MHz, DMSO) δ (ppm)**: –144.10 (sep, $J = 711.1$ Hz, PF₆). **¹⁹F NMR (377 MHz, DMSO) δ (ppm)**: –59.32 (s, $J = 7.4$ Hz), –70.34 (dd, $J = 711.0$, 13.7 Hz). **FT-IR** (ATR) ν (cm⁻¹): 1572 (imine C=N), 1490 (pyridyl C=N). **MP** (°C): 231.2 (decomp.). **MS (HR-ESI, m/z)**: Calculated: 1986.4225, Found: 1986.0101 (20%, [M – PF₆]⁺).

Methyl substituted cationic *N,N*-Ru(II)-*p*-cymene metal complex ([18][PF₆]₃). The ruthenium dimer [Ru(η^6 -*p*-PrⁱC₆H₄Me)Cl₂]₂ (0.0382 g, 0.0624 mmol) was reacted with tris (2-(5-methyl-2-(pyridin-2-yl)-1*H*-benzo[*d*]imidazol-1-yl)ethyl)amine (0.0292 g, 0.0404 mmol) in a at room temperature. NH₄PF₆ (0.0487 g, 0.299 mmol) was added to crude and stirred for 1 h. The desired product ([18][PF₆]₃) was isolated as a bright yellow solid 0.0597 g, 0.0303 mmol. **Yield**: 75.0%. **¹H NMR (400 MHz, DMSO) δ (ppm)**: 9.67–9.53 (m, 3H, H-o), 8.10–7.87 (m, 6H, H-n and H-d), 7.71 (ddd, ²J_{HH} = 28.5 Hz, ³J_{HH} = 16.6 Hz, ⁴J_{HH} = 10.1 Hz, 6H, ArH), 7.54–7.27 (m, 6H, ArH), 6.33 (t, ³J_{HH} = 7.3 Hz, 3H, Ar-*p*-cye), 6.25 (d, ³J_{HH} = 6.0 Hz, 3H, Ar-*p*-cye), 6.15 (dd, ³J_{HH} = 13.2 Hz, ⁴J_{HH} = 6.5 Hz, 3H, Ar-*p*-cye), 6.04 (d, ³J_{HH} = 5.9 Hz, 3H, Ar-*p*-cye), 4.53–4.17 (m, 6H, CH₂), 2.95 (d, ³J_{HH} = 22.9 Hz, 6H, CH₂), 2.65 (s, 3H, CH₃), 2.62 (s, 3H, CH₃), 2.57 (s, 3H, CH₃), 2.39–2.26 (m, 3H, CH(CH₃)₂ *p*-cye), 2.13 (t, ³J_{HH} = 7.1 Hz, 9H, CH₃ *p*-cye), 0.85–0.75 (m, 18H, CH(CH₃)₂ *p*-cye). **¹³C{¹H}-NMR (101 MHz, DMSO) δ (ppm)**: 157.85, 148.01, 145.52, 140.59, 140.23, 136.25, 134.35, 128.58, 127.44, 124.31, 118.31, 112.51, 87.07, 84.72, 82.96, 80.27, 55.35, 53.07, 52.53, 44.24, 30.97, 22.31, 22.10, 21.64, 19.13. **³¹P{¹H}-NMR (162 MHz, DMSO) δ (ppm)**: –144.16 (sep, $J = 711.2$ Hz, PF₆). **FT-IR** (ATR) ν (cm⁻¹): 1674 (imine C=N), 1464 (pyridyl C=N). **MP** (°C): 236.8 (decomp.). **MS (HR-ESI, m/z)**: Calculated: 1823.0329, Found: 1823.1600 (80%, [M – PF₆ + 2H]³⁺).

Mononuclear cationic *N,N*-Ru(II)-*p*-cymene complex [20][PF₆]. 1-Ethyl-2-(pyridin-2-yl)-1*H*-benzo[*d*]imidazole (0.0784 g, 0.352 mmol) was reacted with dichloro(*p*-cymene)

ruthenium(II) dimer (0.107 g, 0.176 mmol) at room temperature for 24 h. NH₄PF₆ (0.0494 g, 0.301 mmol) was added to crude and stirred for 1 h. The desired product ([20][PF₆]) was isolated by vacuum filtration as a yellow solid (0.0899 g, 0.141 mmol). **Yield**: 81.3%. **¹H NMR (300 MHz, DMSO) δ (ppm)**: 9.72 (d, $J = 5.1$ Hz, 1H, ArH), 8.52 (d, $J = 8.1$ Hz, 1H, ArH), 8.36 (t, $J = 7.4$ Hz, 1H, ArH), 8.13 (dd, $J = 6.9$, 1.8 Hz, 1H, ArH), 8.09–8.03 (m, 1H, ArH), 7.90–7.82 (m, 1H, ArH), 7.75–7.62 (m, 2H, ArH), 6.38 (d, $J = 6.1$ Hz, 1H, Ar-*p*-cye), 6.33 (d, $J = 6.2$ Hz, 1H, Ar-*p*-cye), 6.21 (d, $J = 6.1$ Hz, 1H, Ar-*p*-cye), 6.11 (d, $J = 6.1$ Hz, 1H, Ar-*p*-cye), 5.04–4.76 (m, 2H, CH₂CH₃), 2.48–2.38 (m, 1H, CH(CH₃)₂ *p*-cye), 2.24 (s, 3H, CH₃ *p*-cye), 1.43 (t, $J = 7.1$ Hz, 3H, CH₂CH₃), 0.92–0.85 (m, 6H, CH(CH₃)₂ *p*-cye). **¹³C{¹H}-NMR (151 MHz, DMSO) (ppm)**: 157.91, 148.30, 145.64, 140.86, 140.45, 135.78, 127.70, 126.81, 126.02, 125.15, 119.10, 112.88, 104.79, 103.27, 86.90, 84.54, 83.16, 80.57, 40.93, 30.97, 22.13, 22.10, 19.10, 15.19. **MS (HR-ESI, m/z)**: Calculated: 494.0937, Found: 494.0948 (100% [M – PF₆]⁺). **FT-IR** (ATR) ν (cm⁻¹): 1592 (imine C=N), 1493 (pyridyl C=N). **MP** (°C): 186.3 (decomp.).

X-ray structure analysis

Single crystals of **7** and **8** were obtained by slow diffusion of a concentrated solution of **7** or **8** in dichloromethane layered with ethyl acetate, at room temperature over two days. Single-crystal X-ray diffraction data were collected on a Bruker KAPPA APEX II DUO diffractometer using graphite-monochromated MoK α radiation ($\lambda = 0.71073$ Å). Data collection was carried out at 173(2) K. Temperature was controlled by an Oxford Cryostream cooling system (Oxford Cryostat). Cell refinement and data reduction were performed using the program SAINT.⁵⁴ The data were scaled, and absorption correction performed using SADABS.⁵⁵ The structures were solved by direct methods using SHELXS-97⁵³ and refined by full-matrix least-squares methods based on F^2 using SHELXL-2014⁵⁵ and using the graphics interface program X-Seed.⁵⁶ The programs X-Seed and POV-Ray⁵⁶ were used to prepare molecular graphic images. All non-hydrogen atoms were refined anisotropically. All hydrogen atoms were placed in idealised positions and refined in riding models with U_{iso} assigned 1.2 or 1.5 times U_{eq} of their parent atoms and the bond distances were constrained in the range from 0.95 Å to 0.99 Å. CCDC 1940327 (**7**), 1940326 (**8**).†

Cell culture

The human breast adenocarcinoma cell lines, MCF-7 (oestrogen-receptor positive, ER+) was maintained in Roswell Park Memorial Institute (RPMI) 1640 medium (Sigma Aldrich, USA) and the MDA-MB-231 (triple negative, TNBC) was maintained in Dulbecco's Modified Eagle's Medium (DMEM) (Sigma Aldrich, USA). All culture medium was supplemented with 10% heat-inactivated foetal bovine serum (FBS), 100 U mL⁻¹ penicillin and 100 μ g mL⁻¹ streptomycin. The non-tumorigenic human breast epithelial MCF-12A cells were maintained in complete media consisting of DMEM/Ham's F12 supplemented with 10% foetal bovine serum (FBS), 100 U mL⁻¹

penicillin, 0.1 $\mu\text{g ml}^{-1}$ cholera toxin (Sigma, St Louis, MO, USA), 0.5 $\mu\text{g ml}^{-1}$ hydrocortisone (Calbiochem, Billerica, MA), 10 $\mu\text{g ml}^{-1}$ insulin (Novorapid; Novo Nordisk, Copenhagen, Denmark), 20 ng ml^{-1} epidermal growth factor (Gibco, Life Technologies, Carlsbad, CA), and 5% horse serum (Highveld Biological, Lyndhurst, South Africa). Cells were maintained at 37 °C in a 95% air and 5% CO_2 humidified incubator and medium was replaced every 2 to 3 days.

Cytotoxicity studies

For the cytotoxicity assays, MCF-7, MDA-MB-231 breast cancer cells and non-tumorigenic MCF-12A epithelial cells were seeded in a 96-well plate at a density of 4500 cells per well, 3000 cells per well and 6000 cells per well, respectively. The cells were incubated for either 24 (for the MDA-MB-231 cell line) or 48 h (for the MCF-7 and MCF-12A cell lines) to allow adhesion. The cells were then treated with either the vehicle (0.1% DMSO) or 10 μM or 20 μM of the test compounds for 48 h. The impact of the test compounds on cell viability was determined using the 3-(4,5-dimethylthiazol-2-yl)-2,5-diphenyltetrazolium bromide (MTT) assay as described in literature.⁵⁷ The absorbance at 600 nm was determined for each well using a spectrophotometer (GloMax® Explorer Multimode Microplate Reader GM3500, Promega) and normalised to the absorbance of the RPMI medium (for the MCF-7 cell line). To determine the IC_{50} (concentration required to inhibit 50% viability) of selected compounds, the cells were treated with a range of concentrations (5–35 μM). These experiments were performed twice in quadruplicate, and the mean cell viability determined using GraphPad Prism V.5.01 software.

Conflicts of interest

The authors declare no competing financial interest.

Acknowledgements

Financial support from the University of Cape Town and the National Research Foundation (NRF, UID: 114305; 111707) is gratefully acknowledged. We are also thankful for several short term exchange visits between the two laboratories in South Africa and Austria and financial support through the South Africa/Austria Joint Scientific and Technological Cooperation (UID: 106165 and OeAD travel grant ZA01/2017) is gratefully acknowledged.

References

- R. W. Ruddon, *Cancer Biology*, Oxford University Press, 4th edn, 2007.
- CANSA, CANSA: Statistics, <http://www.cansa.org.za/files/2016/08/Fact-Sheet-Cancer-NCR-2011-web-Aug-2016.pdf>, (accessed 20 February 2019).
- WHO, WHO: Cancer, <http://www.who.int/mediacentre/factsheets/fs297/en/>, (accessed 28 June 2018).
- A. Schroeder, D. A. Heller, M. M. Winslow, J. E. Dahlman, G. W. Pratt, R. Langer, T. Jacks and D. G. Anderson, *Nat. Rev. Cancer*, 2011, **12**, 39–50.
- M. Gaba and C. Mohan, *Development of drugs based on imidazole and benzimidazole bioactive heterocycles: Recent advances and future directions*, Springer US, 25th edn, 2016.
- L. Rylands, A. Welsh, K. Maepa, T. Stringer, D. Taylor, K. Chibale and G. S. Smith, *Eur. J. Med. Chem.*, 2019, **161**, 11–21.
- L. T. Wu, Z. Jiang, J. J. Shen, H. Yi, Y. C. Zhan, M. Q. Sha, Z. Wang, S. T. Xue and Z. R. Li, *Eur. J. Med. Chem.*, 2016, **114**, 328–336.
- J. E. Cheong, M. Zaffagni, I. Chung, Y. Xu, Y. Wang, F. E. Jernigan, B. R. Zetter and L. Sun, *Eur. J. Med. Chem.*, 2018, **144**, 372–385.
- C. S. Allardyce and P. J. Dyson, *Dalton Trans.*, 2016, **45**, 3201–3209.
- J. Reedijk, *Eur. J. Inorg. Chem.*, 2009, 1303–1312.
- W. Han and P. J. Dyson, *Eur. J. Inorg. Chem.*, 2006, **20**, 4003–4018.
- E. Alessio, *Eur. J. Inorg. Chem.*, 2017, 1549–1560.
- P. J. Dyson and G. Sava, *Dalton Trans.*, 2006, **16**, 1929–1933.
- C. S. Allardyce, A. Dorcier, C. Scolaro and P. J. Dyson, *Appl. Organomet. Chem.*, 2005, **19**, 1–10.
- I. Kostova, *Curr. Med. Chem.*, 2006, **13**, 1085–1107.
- M. Galanski, V. B. Arion, M. A. Jakupcic and B. K. Keppler, *Curr. Pharm. Des.*, 2003, **9**, 2078–2089.
- G. K. Gransbury, P. Kappen, C. J. Glover, J. N. Hughes, A. Levina, P. A. Lay, I. F. Musgrave and H. H. Harris, *Metallomics*, 2016, **8**, 762–773.
- D. S. Thompson, G. J. Weiss, S. F. Jones, H. A. Burris, R. K. Ramanathan, J. R. Infante, J. C. Bendell, A. Ogden and D. D. Von Hoff, *J. Clin. Oncol.*, 2012, **30**, 3033–3033.
- A. Levina, A. Mitra and P. A. Lay, *Metallomics*, 2009, **1**, 458–470.
- R. Carter, A. Westhorpe, M. J. Romero, A. Habtemariam, C. R. Galleo, Y. Bark and N. Menezes, *Sci. Rep.*, 2016, **6**, 1–12.
- Z. Wang, H. Qian, S. Yiu, J. Sun and G. Zhu, *J. Inorg. Biochem.*, 2014, **131**, 47–55.
- M. Martínez-Alonso, N. Busto, F. A. Jalón, B. R. Manzano, J. M. Leal, A. M. Rodríguez, B. García and G. Espino, *Inorg. Chem.*, 2014, **53**, 11274–11288.
- M. Maroto-Díaz, B. T. Elie, P. Gómez-Sal, J. Pérez-Serrano, R. Gómez, M. Contel and F. J. De Mata, *Dalton Trans.*, 2016, **45**, 7049–7066.
- P. R. Florindo, D. M. Pereira, P. M. Borrhalho, M. P. Rodrigues, M. F. M. Piedade and A. C. Fernandes, *J. Med. Chem.*, 2015, **58**, 4339–4347.
- N. Mohan, S. Muthumari and R. Ramesh, *J. Organomet. Chem.*, 2016, **807**, 45–51.
- P. Govender, B. Therrien and G. S. Smith, *Eur. J. Inorg. Chem.*, 2012, 2853–2862.
- C. Billecke, S. Finnis, L. Tahash, C. Miller, T. Mikkelsen, N. P. Farrell and O. Bögl, *Neuro-Oncology*, 2006, **8**, 215–226.

- 28 P. Govender, N. C. Antonels, J. Mattsson, A. K. Renfrew, P. J. Dyson, J. R. Moss, B. Therrien and G. S. Smith, *J. Organomet. Chem.*, 2009, **694**, 3470–3476.
- 29 A. K. Iyer, G. Khaled, J. Fang and H. Maeda, *Drug Discovery Today*, 2006, **11**, 812–818.
- 30 J. Fang, H. Nakamura and H. Maeda, *Adv. Drug Delivery Rev.*, 2011, **63**, 136–151.
- 31 N. J. Wheate, S. Walker, G. E. Craig and R. Oun, *Dalton Trans.*, 2010, **39**, 8113–8127.
- 32 P. Chellan, K. M. Land, A. Shokar, A. Au, S. H. An, D. Taylor, P. J. Smith, K. Chibale and G. S. Smith, *Organometallics*, 2013, **32**, 4793–4804.
- 33 P. Chellan, K. M. Land, A. Shokar, A. Au, S. H. An, D. Taylor, P. J. Smith, T. Riedel, P. J. Dyson, K. Chibale and G. S. Smith, *Dalton Trans.*, 2014, **43**, 513–526.
- 34 B. C. E. Makhubela, M. Meyer and G. S. Smith, *J. Organomet. Chem.*, 2014, **772–773**, 229–241.
- 35 A. R. Burgoyne, C. H. Kaschula, M. I. Parker and G. S. Smith, *J. Organomet. Chem.*, 2017, **846**, 100–104.
- 36 I. Cassells, T. Stringer, A. T. Hutton, S. Prince and G. S. Smith, *J. Biol. Inorg. Chem.*, 2018, **23**, 763–774.
- 37 A. R. Burgoyne, C. H. Kaschula, M. I. Parker and G. S. Smith, *Eur. J. Inorg. Chem.*, 2016, 1267–1273.
- 38 F. Bray, J. Ferlay and I. Soerjomataram, *Ca-Cancer J. Clin.*, 2018, **68**, 394–424.
- 39 B. Arslan, C. Kazak, H. Karataş and S. Özden, *Acta Crystallogr., Sect. E: Struct. Rep. Online*, 2004, **60**, 1535–1537.
- 40 N. Dalla-Favera, L. Guénée, G. Bernardinelli and C. Piguet, *J. Chem. Soc., Dalton Trans.*, 2009, 7625–7638.
- 41 E. J. Hennessy, V. Oza, A. Adam, K. Byth, L. Castriotta, G. Grewal, G. A. Hamilton, V. M. Kamhi, P. Lewis, D. Li, P. Lyne, L. Öster, M. T. Rooney, J. C. Saeh, L. Sha, Q. Su, S. Wen, Y. Xue and B. Yang, *J. Med. Chem.*, 2015, **58**, 7057–7075.
- 42 L. Huang, K. Z. Wang, C. H. Huang, F. Y. Li and Y. Y. Huang, *J. Mater. Chem.*, 2001, **11**, 790–793.
- 43 Z. Y. Zhou, J. C. Zhang, N. X. Li and C. M. Zhang, *Acta Crystallogr., Sect. E: Struct. Rep. Online*, 2009, **65**, 3019–3021.
- 44 *Handbook of Anticancer Pharmacokinetics and Pharmacodynamics*, ed. M. A. Rudek, C. A. Chau, W. Figg and H. L. McLeod, Humana Press, Totowa, 2nd edn, 2014.
- 45 Y. Mizumura, Y. Matsumura, T. Hamaguchi, N. Nishiyama, K. Kataoka, T. Kawaguchi, W. J. M. Hrushesky, F. Moriyasu and T. Kakizoe, *Jpn. J. Cancer Res.*, 2001, **92**, 328–336.
- 46 D. L. Holliday and V. Speirs, *Breast Cancer Res.*, 2011, **13**, 215–222.
- 47 A. Zaim, M. Pauzi, S. K. Yeap, N. Abu, K. L. Lim, A. R. Omar, S. A. Aziz, A. Leow, T. Chow, T. Subramani and S. G. Tan, *Chin. Med.*, 2016, **46**, 1–11.
- 48 R. F. S. Lee, A. Meibom, G. Sava, C. Maclachlan, G. W. Knott and P. J. Dyson, *Int. J. Mol. Sci.*, 2017, **2**, 1869–1877.
- 49 P. Rogala, A. Jabłońska-Wawrzycka, K. Kazimierzczuk, A. Borek, A. Błażejczyk, J. Wietrzyk and B. Barszcz, *J. Mol. Struct.*, 2016, **1126**, 74–82.
- 50 P. Elumalai, Y. J. Jeong, D. W. Park, D. H. Kim, H. Kim, S. C. Kang and K. W. Chi, *Dalton Trans.*, 2016, **45**, 6667–6673.
- 51 M. A. Bennett and A. K. Smith, *Dalton Trans.*, 1974, 233–241.
- 52 R. Hernández-Sánchez, A. M. Willis, S. L. Zheng and T. A. Betley, *Angew. Chem., Int. Ed.*, 2015, **54**, 12009–12013.
- 53 A. Bruker and A. X. S. Saint, *Acta Crystallogr., Sect. A: Found. Crystallogr.*, 2008, **64**, 112–122.
- 54 G. M. Sheldrick, *SHELXL-97, Program for X-Ray Crystal Structure Refinement*, 1997.
- 55 L. J. Barbour, *J. Supramol. Chem.*, 2001, **1**, 198–191.
- 56 <http://www.povray.org>.
- 57 T. Mosmann, *J. Immunol. Methods*, 1983, **65**, 55–63.